Supplementary Material

3D Printing MXene-Based Film and Cellulose Nanofiber Reinforced Hydrogel Electrolyte to Enable High-Performance Flexible Supercapacitor

Guoqiang Zhou[a,†], Xinyue Liu[a,†], Chaozheng Liu[a], Zhenglin Li[a], Chuhang Liu[a], Xiaojie Shi[a], Ziyan Li[b], Changtong Mei[a,*], and Mei-Chun Li[a,b,c,*]

[a]Co-Innovation Center of Efficient Processing and Utilization of Forest Resources, College of Materials Science and Engineering, Nanjing Forestry University, Nanjing 210000, China

[b]School of Petroleum Engineering, China University of Petroleum (East China), Qingdao, Shandong 266580, China

[c]Key Laboratory of Unconventional Oil & Gas Development (China University of Petroleum (East China)), Ministry of Education, Qingdao, Shandong 266580, China

[†]Zhou and Liu contributed equally to this work

Corresponding Authors*

Changtong Mei: mei@njfu.edu.cn

Mei-Chun Li: mli@upc.edu.cn

Experimental Section

Preparation of PAM/CNF hydrogel electrolyte

Hydrogel electrolyte was prepared using the in situ radical polymerization approach combined with electrolyte impregnation treatment according to previous works.[1, 2] Detailly, 3g acrylamide (AM) monomer, 0.02 g ammonium persulfate (APS) initiator, and 2 mg N, N'-methylenebisacrylamide (MBAA) cross-linking agent were added into the 10 g 1 wt% CNF suspension with vigorous stirring for 60 min at room temperature. Subsequently, the hybrid suspension was kept in a vacuum oven at 25 ℃ for 10 min to eliminate the bubbles. Then, the hybrid suspension was decanted to a mold with a thickness of 0.7 mm and kept at 60℃ for 60 min to proceed the in situ radical polymerization, and the PAM/CNF hydrogel was obtained after polymerization. The as-prepared PAM/CNF hydrogel was immersed in 1 M H_2SO_4 aqueous solution at room temperature for 24 h to produce the hydrogel electrolyte. For comparison, pure PAM hydrogel electrolyte was prepared by replacing the CNF suspension with deionized water, and the other procedures were same.

Measurement of ionic conductivity

The ionic conductivity of the hydrogel electrolyte was obtained from the electrochemical impedance spectroscopy (EIS) using the following equation [3]:

$$\sigma = \frac{d}{R \cdot S} \qquad (1)$$

Where σ is the ionic conductivity ($mS \cdot cm^{-1}$), d and S is the thickness and area of the hydrogel electrolyte sample, respectively. R is the intercept of the EIS curve at X-axis (Ω). The PAM and PAM/CNF hydrogel electrolyte were pressed into the wafer shape with a radius of 0.8 cm using the stainless-steel mold, thus the area of the hydrogel electrolyte sample was 2.01 cm^{-2}. The thickness of PAM and PAM/CNF hydrogel electrolyte sample were 1.23 and 1.35 mm,

respectively. To conduct the EIS measurement, two titanium foils were utilized as collector and attached to both side of the electrolyte sample. Then, the tests were performed over the frequency range of 10^5 to 10^{-2} Hz with a potential amplitude of 5 mV at room temperature using a CHI760E electrochemical workstation.

Preparation of Ti3C2Tx MXene nanosheets

$Ti_3C_2T_x$ MXene was synthesized using the chemical etching approach combined with ultrasonic treatment as reported previously.[4] In brief, 2 g Ti_3AlC_2 MAX were added to the 40 mL HCl/LiF hybrid solution with stirring for 24 h at 35 ℃ to etch the Al. The HCl/LiF hybrid solution was prepared by dissolving 2.4 g LiF in 40 mL 9M HCl solution. After reaction, the multilayer $Ti_3C_2T_x$ sediment was washed by deionized (DI) water and centrifuged several times (3500 rpm) until the pH of supernatant became ~6. The multilayer $Ti_3C_2T_x$ was carefully collected and dispersed in 200 mL DI water, followed by ultrasonic treated at 200 W for 30 min to exfoliate the nanosheets. Finally, the suspension was configured at 3500 rpm for 30 min, and the dark green supernatant containing the $Ti_3C_2T_x$ nanosheets was obtained.**Formulation of $Ti_3C_2T_x$/CNF/MWCNT (MXM) gel ink**

First, CNFs were derived from the waste oil palm wood trunk according to previous works.[5] Then, carboxylated MWCNTs were added to the CNF suspension (0.2 wt%) with continuous stirring, and the mass ratio of CNF and MWCNT was 1:2. After stirring for 30 min, the CNF/MWCNT hybrid suspension were ultrasonic treated for 1 h with the power of 300 W in an ice bath to keep the MWCNT evenly dispersed in the suspension.

The CNF/MWCNT suspension was mixed with the $Ti_3C_2T_x$ suspension in a solid mass ratio of 3:7, then the hybrid suspension was ultrasonic treated for 10 min (100 W) to ensure the

dispersion uniformity of each component. The hybrid CNF/MWCNT/$Ti_3C_2T_x$ suspension was concentrated to a solid content of 6 wt% using the highly hydrophilic absorbent beads, which is detailed in previous study.[6] After homogenization treatment by a vacuum planetary high-speed mixer, a homogenous MXM gel ink was obtained. As a control, pure $Ti_3C_2T_x$ ink with a concentration of 6 wt% was also prepared under the same protocol as the MXM gel ink.

Rheology Measurement

The rheological properties of MXM and $Ti_3C_2T_x$ inks were studied by a MARS60 rheometer (Thermo Fisher, Germany) with a 35 mm parallel plate at temperature of 25 ℃. The steady shearing tests were carried out at the shear rates ranging from 10^{-2} to 10^3 s^{-1} to record the change in viscosity. For the thixotropy measurement, the viscosity over time was recorded when applying the alternating shear rates (10^{-2} & 10^2 s^{-1}). The dynamic stress sweep measurement was performed to test the storage modulus and loss modulus as a function of stress at a frequency of 1Hz. And the dynamic angular frequency sweep of gel ink was conducted in the frequency range of 1 to 10^2 rad·s^{-1} at stress of 1 Pa.

3D printing of $Ti_3C_2T_x$/CNF/MWCNT (MXM) gel ink

3D printing of MXM gel ink was carried out using a Dr. INVIVO 4D bioprinter (ROKIT Healthcare, INC, South Korea). The MXM ink was loaded into the printing cylinder and configured at 2000 rpm for 3 min. Then, using an air-powered dispenser as the pressure source, the MXM gel filaments were extruded on the glass substrate at different printing speeds (2, 3, 4, 5 mm·s^{-1}) at the pressure of 28 KPa. The printing speed were optimized by comparing the actual width of the filament with the diameter of the nozzle (0.4 mm). Before 3D printing, the 3D structural models were designed using the 3D MAX software, which was subsequently

transformed into the G-code instructions by a Newcreator software associated with the 3D printer. Using the optimal printing speed, different gel architectures were printed in layer-by-layer on the glass substrate by executing the corresponding G-codes at the temperature of 25 ℃. To achieve the flexible 3D printed MXM film, the MXM ink was printed on the hydrophobic PP substrate, and dry at the room temperature for 24 h.

3D printing and assembly of flexible supercapacitor

Two interdigitated MCM gel architectures with two layers (0.4 mm) were printed on the hydrophilic PTFE substrate, and left to dry at room temperature to form the interdigitated film electrodes that could adhere onto the substrate (MXM@PTFE). The designed interdigitated model was schematically shown in Figure in Supporting information. For the preparation of PAM/CNF hydrogel based quasi solid electrolyte, the in-situ polymerization strategy and impregnation of electrolyte were employed, which is detailed in Supporting information. The as-prepared PAM/CNF hydrogel electrolyte was covered on the interdigitated MXM film electrodes, and two conductive copper foil tapes were connected separately with two electrodes. Finally, the above flexible SC device was encapsulated in polyethylene film by hot lamination.

Characterization

The Zeta potential values were measured by a ZetaTrac analyzer (Microtrac, Largo, USA). The morphologies of the samples were observed by using the transmission electron microscope (TEM, JEM-1400, JEOL), and a filed-emission scanning microscope (FE-SEM, JSM-7600F, JEOL) with an energy dispersive X-ray spectroscopy (EDS). The width of extruded filament was measured by the Image J software according to the ruler. X-ray patterns of the MXene and TCM film were recorded using an X-ray diffraction (XRD, Ultima IV, Japan) with the Cu Kα radiation,

and the tests were performed at 40 kV and 40 Ma. Micrometritics ASAP 2020 analyzer was used to measure the N_2 adsorption/desorption isotherms, and the pore size distribution and specific surface area of the samples were obtained according to the DFT and BET method, respectively. The wettability of the samples was evaluated using the contact angle testing instrument (DSA100S, German Dataphysics). Resistance of the film after and before bending was recorded using an Avometer. Chemical structure of the CNF, PAM, PAM/CNF was characterized by a Fourier transform infrared (FTIR) spectrometer (VERTEX 80v, Germany Bruker). A Universal Testing Machine (Instron 5966, USA) was used to record the tensile stress-strain curves of the PAM and PAM/CNF hydrogel at room temperature. Linear voltammetry curve of the sample was obtained using the electrochemical workstation (CHI 760E, China) in two-electrode configuration. The measurements of the ionic conductivity and the electrochemical performance are detailed in Supporting information.

Electrochemical Measurements

The electrochemical performance of the 3D printed MCM film was firstly measured in a three-electrode configuration with 1 M H_2SO_4 as electrolyte using the electrochemical working station. In the three-electrode system, the MCM film, mercury/mercurous sulfate electrode, and platinum sheet electrode were used as the working electrode, reference electrode, and counter electrode, respectively. For the 3D printed symmetric supercapacitor device, the electrochemical performance was tested by applying a three-electrode configuration, and the geometric area of active MCM film-based electrode was set as 1.376 cm^{-2}, as shown in Fig. S20. Cyclic voltammetry (CV), Galvanostatic charge-discharge (GCD) tests were carried out at room temperature to evaluate the electrochemical performance and capacitive behavior. The EIS test

was performed at an open circuit voltage and under a potential amplitude of 5 mV in 10^5 to 10^{-2} Hz. Long-term cycling stability was evaluated by repeating the GCD tests at a current density of 20 $mA \cdot cm^{-2}$, and the corresponding areal capacitance retention was recorded. The areal capacitance of MCM film and device was calculated using the following equation according to the GCD curves at different current densities:

$$C_S = \frac{I \cdot t}{\Delta U \cdot S} \quad (2)$$

where C_S is the areal capacitance ($mF \cdot cm^{-2}$), I is the applied charge-discharge current (mA), t is the discharging time (s), ΔU is the potential change in GCD curve (V), and S is area of the active TCM film (cm^{-2}). The CV profile at 5 $mV \cdot s^{-1}$ and GCD curve at 1 $mA \cdot cm^{-2}$ of the device at different bending states or after various bending cycles were measured to evaluate the capacitive stability.

The energy density and power density of the device were obtained according to the following equation:

$$E = 0.5 \cdot C_S \cdot (\Delta U)^2 \quad (3)$$

$$P = \frac{3600 \cdot E}{t} \quad (4)$$

Where E ($\mu Wh \cdot cm^{-2}$) and P ($mW \cdot cm^{-2}$) are the energy density and power density, respectively. C_S is the capacitance obtained from equation (2).

Figures

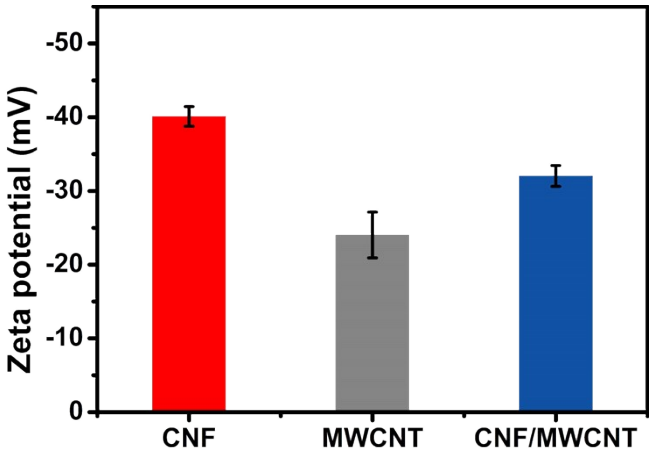

Fig. S1 Zeta potential value of CNF and CNF/MWCNT suspension

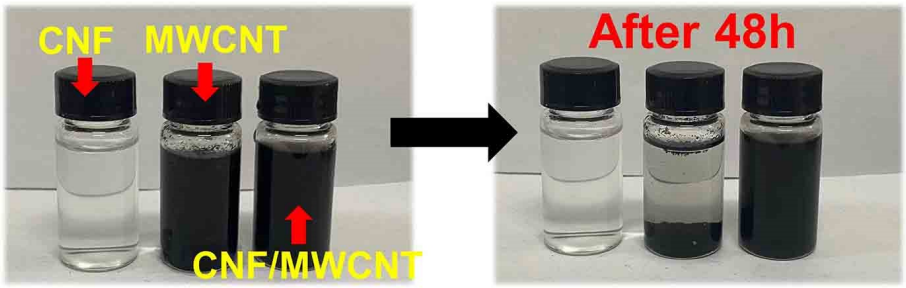

Fig. S2 Digital images of CNF, MWCNT and CNF/MWCNT suspension before and after standing for 48 h

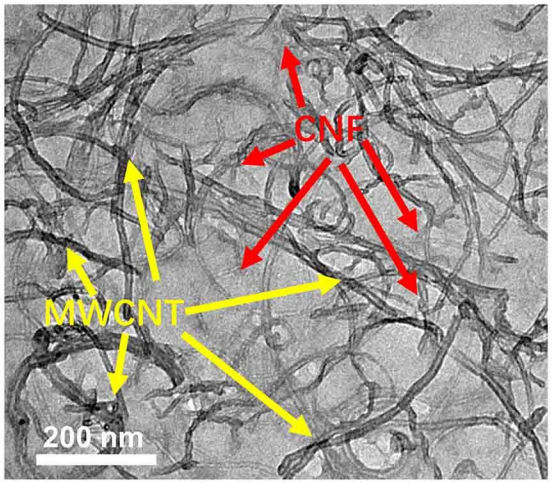

Fig. S3 TEM image of CNF/MWCNT, showing the physically entangled network

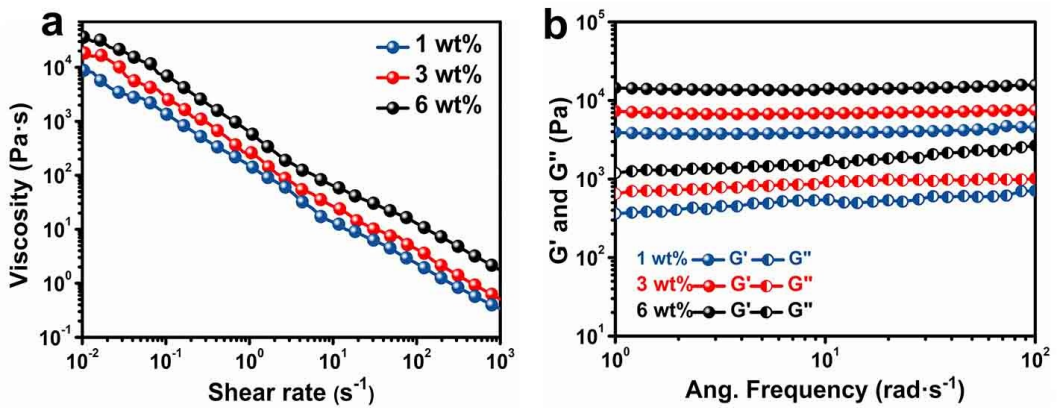

Fig. S4 (a) Viscosity as a function of shear rate of CNF/MWCNT suspensions with different concentrations. (b) G′ and G″ as a function of angular frequency

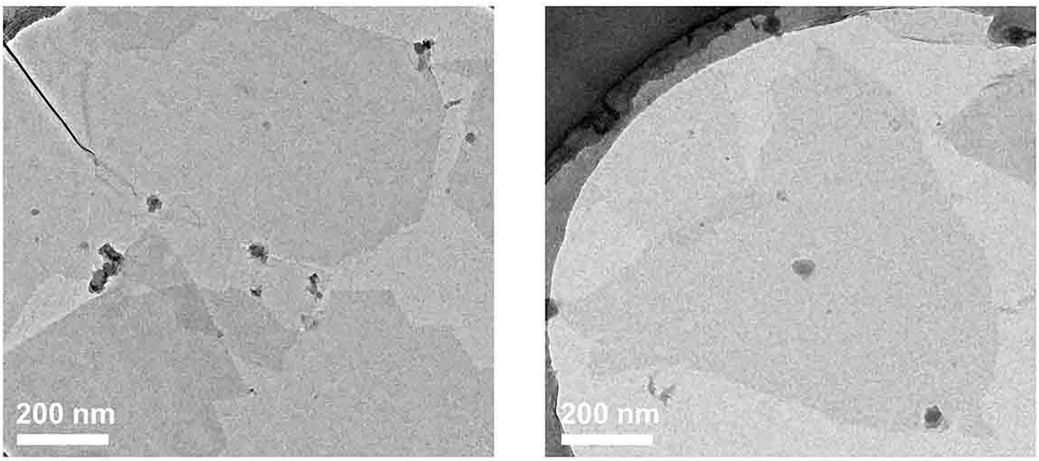

Fig. S5 TEM image of MXene nanosheets

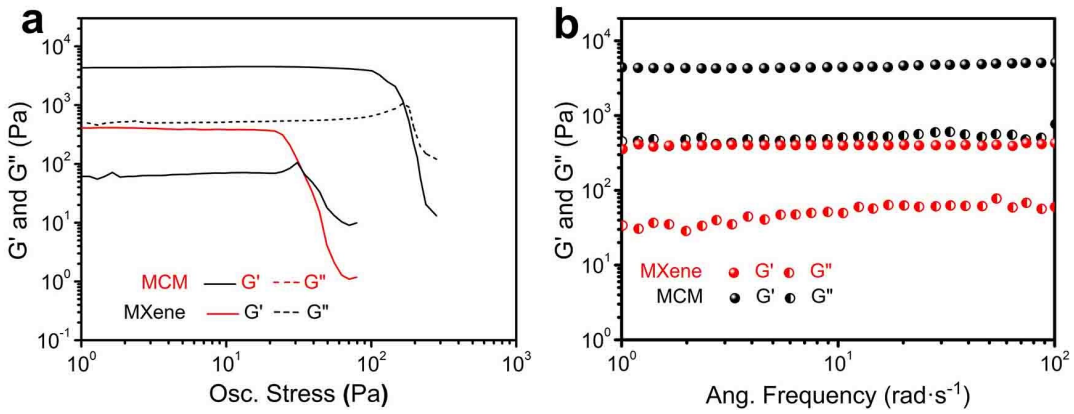

Fig. S6 G′ and G″ as a function of (a) oscillatory stress and (b) angular frequency

Fig. S7 Digital images and the corresponding width of the extruded filament at different printing speeds

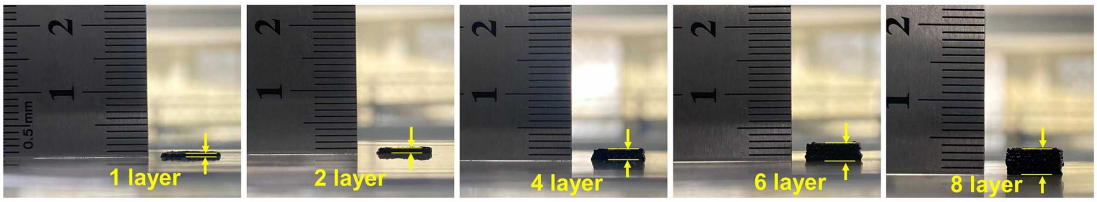

Fig. S8 Digital images of the printed gel block with different layers

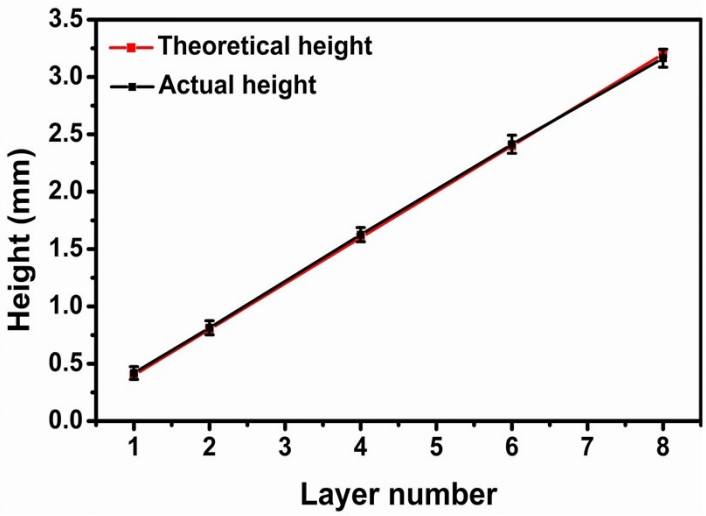

Fig. S9 The actual- and theoretical-height of 3D printed gel blocks with different layers. Note

the theoretical value is the height of block model

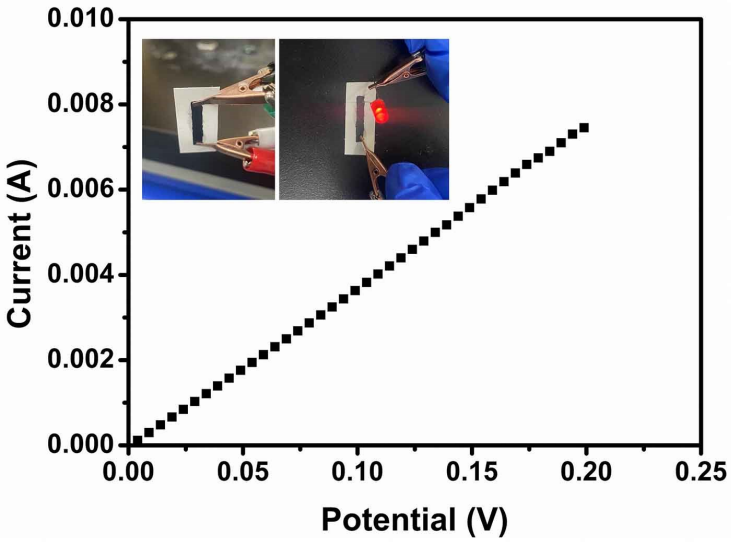

Fig. S10 Linear voltammetry curve of the MCM film on a PTFE substrate. Left inset is the test method, and the right inset shows that the LED is illuminated when it was touched the MCM film in circuit

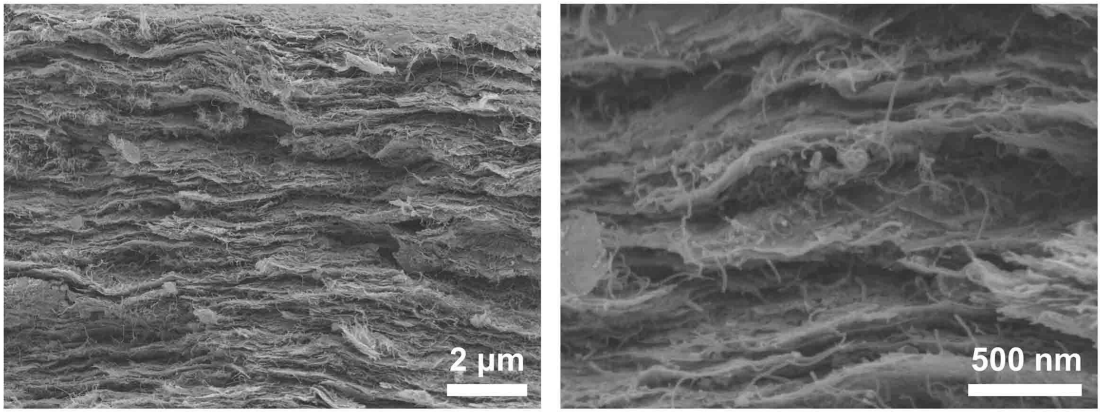

Fig. S11 Cross-sectional view SEM images of MCM film

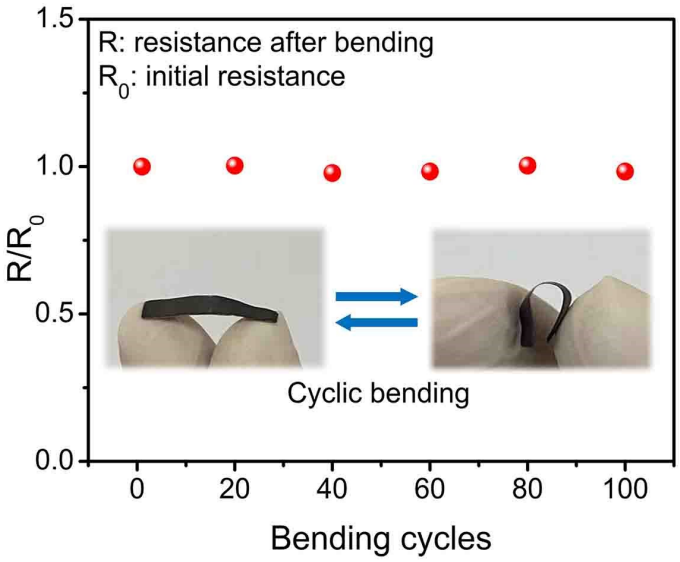

Fig. S12 Relative resistance of MCM film after different bending cycles

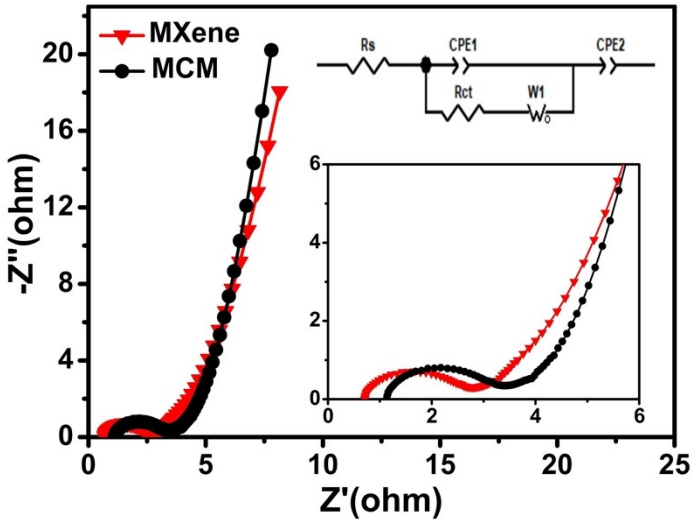

Fig. S13 EIS plot of MCM and MXene film in three-electrode system, insets are the enlarged plots at the high-frequency range and equivalent circuit diagram

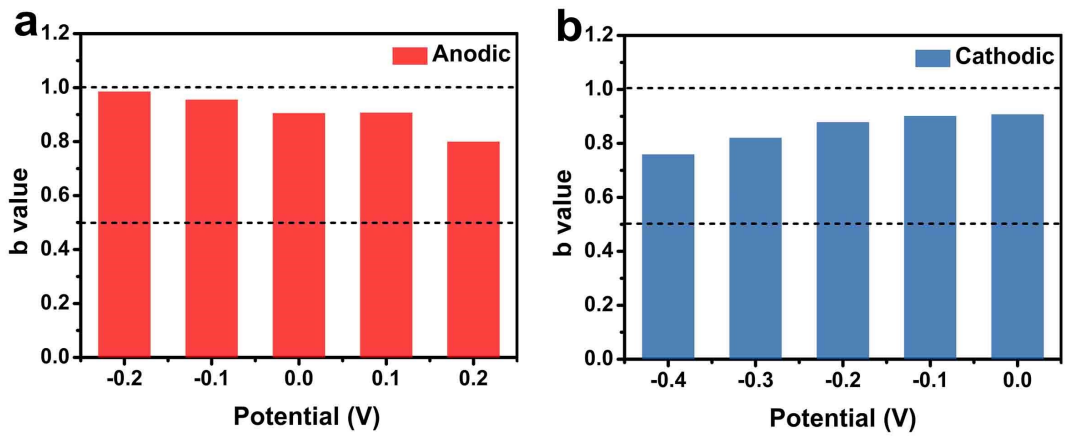

Fig. S14 (a) cathodic and (b) anodic b-value at different potentials in the CV profiles

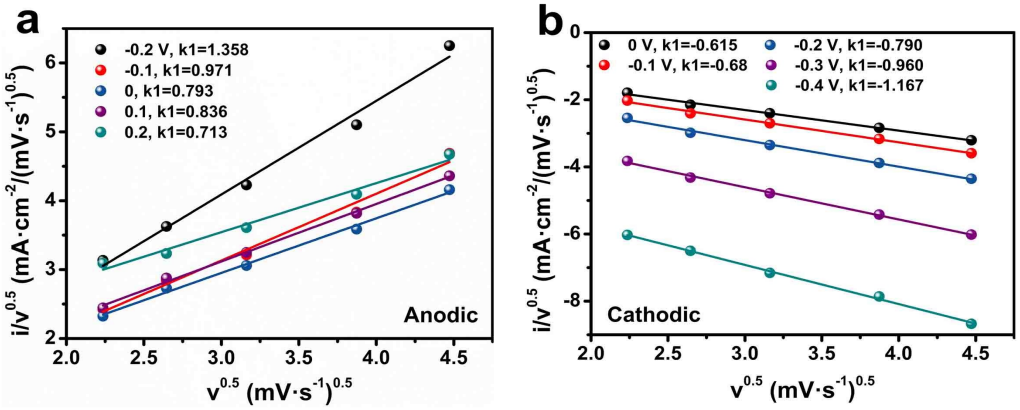

Fig. S15 Linear relationship between the (a) anodic current and (b) cathodic current response to the square root of the scan rate and square root of scan rate at a given potential.

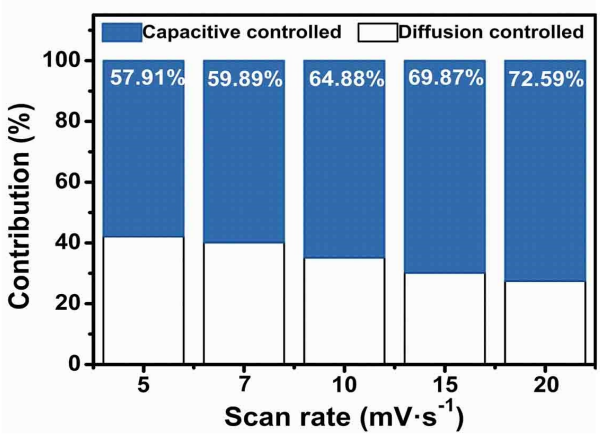

Fig. S16 Capacitive- and diffusion-controlled contribution rate

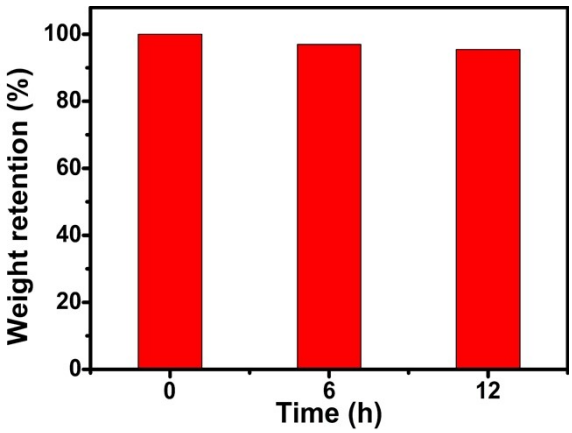

Fig. S17 Weight retention of PAM/CNF hydrogel electrolyte in polyethylene film

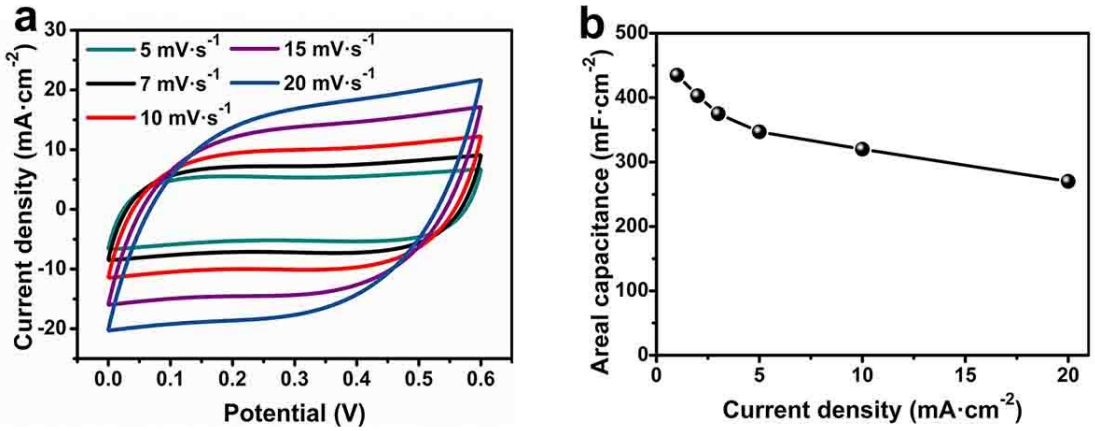

Fig. S18 (a) CV profiles at different scan rates and (b) areal capacitance at different current densities of the FSC.

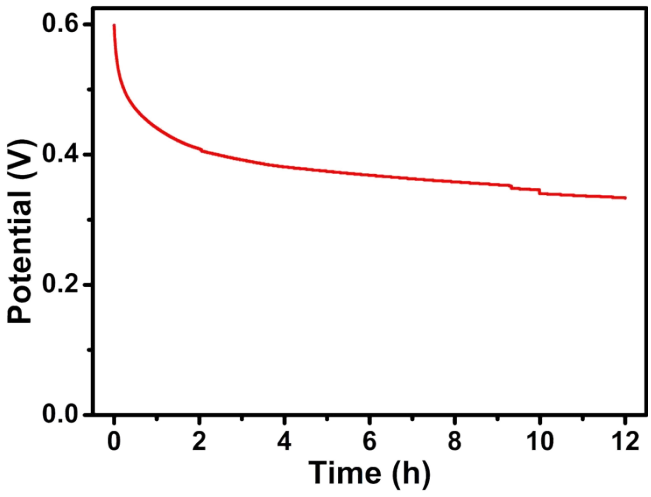

Fig. S19 The potential of device as a function of time

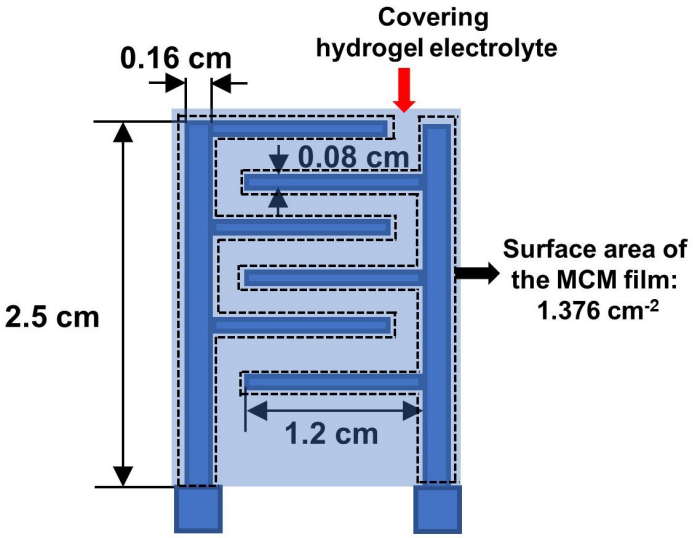

Fig. S20 Schematic diagram of device area calculation

Tables

Table S1. Comparison on areal capacitance of 3D printed MCM film and other previously reported flexible electrodes

Electrode material	Electrolyte	Capacitance	Reference
$Ti_3C_2T_x$/MWCNT/CNF	1M H_2SO_4	1.13 $F \cdot cm^{-2}$@1mA$\cdot cm^{-2}$	This work
$Ti_3C_2T_x$/CNF	3M H_2SO_4	0.568 $F \cdot cm^{-2}$@2mV$\cdot s^{-1}$	7
$Ti_3C_2T_x$/Ag NP	1M Na_2SO_4	1.173 $F \cdot cm^{-2}$@5mA$\cdot cm^{-2}$	8
macroporous $Ti_3C_2T_x$	1M H_2SO_4	1.025 $F \cdot cm^{-2}$@2mV$\cdot s^{-1}$	9
Heat treated $Ti_3C_2T_x$@wood	3M H_2SO_4	0.935 $F \cdot cm^{-2}$@0.2mA$\cdot cm^{-2}$	10
porous $Ti_3C_2T_x$/CNT film	3M H_2SO_4	0.6 $F \cdot cm^{-2}$@5mV$\cdot s^{-1}$	11
PPy/l-$Ti_3C_2T_x$	0.5M H_2SO_4	0.203 $F \cdot cm^{-2}$@1mA$\cdot cm^{-2}$	12
MXene/CAC	3M H_2SO_4	0.433 $F \cdot cm^{-2}$@1A$\cdot g^{-1}$	13
$Ti_3C_2T_x$/MWCNT/PC	6M KOH	0.364 $F \cdot cm^{-2}$@0.1mA$\cdot cm^{-2}$	14
$Ti_3C_2T_x$/BC	PVA/H_2SO_4	0.112 $F \cdot cm^{-2}$@1mA$\cdot cm^{-2}$	15
$Ti_3C_2T_x$/CNF-PEI	3M H_2SO_4	0.139 $F \cdot cm^{-2}$@0.2mA$\cdot cm^{-2}$	16
d-$Ti_3C_2T_x$@NF	1M KOH	0.246 $F \cdot cm^{-2}$@5mV$\cdot s^{-1}$	17
PPy/RGO/M-PEFT	1M Na_2SO_4	1.17 $F \cdot cm^{-2}$@1mA$\cdot cm^{-2}$	18
CNTs/cotton	1M $LiPF_6$	0.48 $F \cdot cm^{-2}$@0.2mA$\cdot cm^{-2}$	19
AC/Cotton	1M Na_2SO_4	0.43 $F \cdot cm^{-2}$@5mV$\cdot s^{-1}$	20

Table S2. Comparison on areal capacitance of MXene-based FSC between this work and previously reported studies

FSC type	Electrolyte	Capacitance	Reference
$Ti_3C_2T_x$/MWCNT/CNF	PAM/CNF/ H_2SO_4	435 $mF \cdot cm^{-2}$@1$mA \cdot cm^{-2}$	This work
MXene-rGO	PVA/H_3PO_4	372.2 $mF \cdot cm^{-2}$@10$mV \cdot s^{-1}$	21
Carbonized MXene/Cotton fabric	PVA/H_3PO_4	500.8 $mF \cdot cm^{-2}$@0.5$mA \cdot cm^{-2}$	22
porous $Ti_3C_2T_x$/CNT film	3M H_2SO_4	118 $mF \cdot cm^{-2}$@5$mV \cdot s^{-1}$	11
$Ti_3C_2T_x$ /SnS_2/CNF	PVA/H_2SO_4	226 $mF \cdot cm^{-2}$@0.8 $mA \cdot cm^{-2}$	23
$Ti_3C_2T_x$/MWCNT/PC	PVA/KOH	212 $mF \cdot cm^{-2}$@0.1 $mA \cdot cm^{-2}$	14
MXene-Coated Activated Carbon Cloth	PVA/H_2SO_4	413 $mF \cdot cm^{-2}$@0.5$mA \cdot cm^{-2}$	24
$Ti_3C_2T_x$/CNF/PC	PVA/H_2SO_4	143 $mF \cdot cm^{-2}$@@0.5$mA \cdot cm^{-2}$	25
CT-Ti_3C_2@V_2O_5	PVA/LiCl	477 $mF \cdot cm^{-2}$@1$mV \cdot s^{-1}$	26
d-$Ti_3C_2T_x$@NF	PVA/KOH	166 $mF \cdot cm^{-2}$@0.2$A \cdot g^{-1}$	17
Heat treated $Ti_3C_2T_x$@wood	3M H_2SO_4	302 $mF \cdot cm^{-2}$@0.5$mA \cdot cm^{-2}$	10
$Ti_3C_2T_x$ @Modified carbon cloth	1M H_2SO_4	513 $mF \cdot cm^{-2}$@2$mV \cdot s^{-1}$	27

Table S3. Comparison on energy- and power-density of MXene-based FSC between this work and previously reported studies

FSC type	Electrolyte	Energy density (Power density)	Reference
$Ti_3C_2T_x$/MWCNT/CNF	PAM/CNF/ H_2SO_4	21.7 μWh·cm^{-2}@0.3 mW·cm^{-2}	This work
Stamped MXene	PVA/H_2SO_4	0.72 μWh·cm^{-2}@0.015 mW·cm^{-2}	28
3D printed MXene	PVA/H_2SO_4	8.4 μWh·cm^{-2}@0.102 mW·cm^{-2}	6
3D printed MXene	PVA/H_2SO_4	24.4 μWh·cm^{-2}@0.27 mW·cm^{-2}	29
3D printed MXene aerogel	PVA/H_2SO_4	3.9 μWh·cm^{-2}@0.05 mW·cm^{-2}	30
$Ti_3C_2T_x$ fiber	PVA/H_2SO_4	7.3 μWh·cm^{-2}@0.132 mW·cm^{-2}	31
$Ti_3C_2T_x$/MWCNT/PC	PVA/KOH	10.5 μWh·cm^{-2}@0.0298 mW·cm^{-2}	14
$Ti_3C_2T_x$/graphene aerogel	PVA/H_2SO_4	2.18 μWh·cm^{-2}@0.06 mW·cm^{-2}	32
Transparent MXene	PVA/ H_2SO_4	0.05 μWh·cm^{-2}@0.0024 mW·cm^{-2}	33

References

1. X. Li, L. Yuan, R. Liu, H. He, J. Hao, Y. Lu, Y. Wang, G. Liang, G. Yuan and Z. Guo, *Adv Energy Mater*, 2021, **11**, 2003010.
2. G. Zhou, M.-C. Li, C. Liu, W. Chen, G. Yu, D. Zhang, Z. Li and C. Mei, *Ind Crop Prod*, 2023, **193**, 116216.
3. C. Liu, Z. Li, X. Zhang, W. Xu, W. Chen, K. Zhao, Y. Wang, S. Hong, Q. Wu and M. C. Li, *Adv Sci*, 2022, **9**, 2202380.
4. W. T. Cao, C. Ma, D. S. Mao, J. Zhang, M. G. Ma and F. Chen, *Adv Funct Mater*, 2019, **29**.
5. G. Zhou, M. C. Li, C. Liu, Q. Wu and C. Mei, *Adv Funct Mater*, 2022, **32**, 2109593.
6. J. Orangi, F. Hamade, V. A. Davis and M. Beidaghi, *Acs Nano*, 2019, **14**, 640-650.
7. W. Q. Tian, A. VahidMohammadi, M. S. Reid, Z. Wang, L. Q. Ouyang, J. Erlandsson, T.

Pettersson, L. Wagberg, M. Beidaghi and M. M. Hamedi, *Adv Mater*, 2019, **31**.

8. L. Li, N. Zhang, M. Y. Zhang, L. Wu, X. T. Zhang and Z. G. Zhang, *Acs Sustain Chem Eng*, 2018, **6**, 7442-7450.

9. X. F. Zhang, X. D. Liu, R. Z. Yan, J. Q. Yang, Y. Liu and S. L. Dong, *J Mater Chem C*, 2020, **8**, 2008-2013.

10. D. Zhang, K. Yang, T. Zhang, M. Luo, M. Li, Z. Li, C. Liu, Y. Ling, W. Chen and X. Zhou, *Chem Eng J*, 2023, **460**, 141733.

11. P. Zhang, Q. Z. Zhu, R. A. Soomro, S. Y. He, N. Sun, N. Qiao and B. Xu, *Adv Funct Mater*, 2020, **30**.

12. M. S. Zhu, Y. Huang, Q. H. Deng, J. Zhou, Z. X. Pei, Q. Xue, Y. Huang, Z. F. Wang, H. F. Li, Q. Huang and C. Y. Zhi, *Adv Energy Mater*, 2016, **6**.

13. P. Zhang, J. P. Li, D. Y. Yang, R. A. Soomro and B. Xu, *Adv Funct Mater*, 2023, **33**.

14. K. Yang, M. Luo, D. Zhang, C. Liu, Z. Li, L. Wang, W. Chen and X. Zhou, *Chem Eng J*, 2022, **427**, 132002.

15. S. Q. Jiao, A. G. Zhou, M. Z. Wu and H. B. Hu, *Adv Sci*, 2019, **6**.

16. G. Zhou, X. Wang, T. Wan, C. Liu, W. Chen, S. Jiang, J. Han, Y. Yan, M. C. Li and C. Mei, *Energy Environ Mater*, 2022, e12454.

17. S. Xu, G. Wei, J. Li, Y. Ji, N. Klyui, V. Izotov and W. Han, *Chem Eng J*, 2017, **317**, 1026-1036.

18. X. Li, R. Liu, C. Xu, Y. Bai, X. Zhou, Y. Wang and G. Yuan, *Adv Funct Mater*, 2018, **28**, 1800064.

19. L. B. Hu, M. Pasta, F. La Mantia, L. F. Cui, S. Jeong, H. D. Deshazer, J. W. Choi, S. M. Han and Y. Cui, *Nano Lett*, 2010, **10**, 708-714.

20. K. Jost, C. R. Perez, J. K. McDonough, V. Presser, M. Heon, G. Dion and Y. Gogotsi, *Energ Environ Sci*, 2011, **4**, 5060-5067.

21. Q. Yang, Z. Xu, B. Fang, T. Huang, S. Cai, H. Chen, Y. Liu, K. Gopalsamy, W. Gao and C. Gao, *J Mater Chem A*, 2017, **5**, 22113-22119.

22. Y. Li, Z. Lu, B. Xin, Y. Liu, Y. Cui and Y. Hu, *Applied Surface Science*, 2020, **528**, 146975.

23. C. Cai, W. Zhou and Y. Fu, *Chem Eng J*, 2021, **418**, 129275.

24. L. Wang, D. N. Shao, J. Y. Guo, S. Y. Zhang and Y. Lu, *Energy Technol-Ger*, 2020, **8**.

25. W. M. Chen, D. T. Zhang, K. Yang, M. Luo, P. Yang and X. Y. Zhou, *Chem Eng J*, 2021, **413**.

26. Z. Z. Zhang, M. Guo, Y. H. Tang, C. B. Liu, J. Zhou, J. L. Yuan and J. Y. Gu, *Nanotechnology*, 2020, **31**.

27. Y. Li, B. J. Xin, Z. Lu, X. Zhou, Y. Liu and Y. X. Hu, *Int J Energ Res*, 2021, **45**, 9229-9240.

28. C. F. Zhang, M. P. Kremer, A. Seral-Ascaso, S. H. Park, N. McEvoy, B. Anasori, Y. Gogotsi and V. Nicolosi, *Adv Funct Mater*, 2018, **28**.

29. W. J. Yang, J. Yang, J. J. Byun, F. P. Moissinac, J. Q. Xu, S. J. Haigh, M. Domingos, M. A. Bissett, R. A. W. Dryfe and S. Barg, *Adv Mater*, 2019, **31**.

30. H. Tetik, J. Orangi, G. Yang, K. R. Zhao, S. Bin Mujib, G. Singh, M. Beidaghi and D. Lin, *Adv Mater*, 2022, **34**.

31. M. M. Hu, Z. J. Li, G. X. Li, T. Hu, C. Zhang and X. H. Wang, *Advanced Materials Technologies*, 2017, **2**.

32. Y. Yue, N. Liu, Y. A. Ma, S. L. Wang, W. J. Liu, C. Luo, H. Zhang, F. Cheng, J. Y. Rao, X. K. Hu, J. Su and Y. H. Gao, *Acs Nano*, 2018, **12**, 4224-4232.

33. C. F. Zhang, B. Anasori, A. Seral-Ascaso, S. H. Park, N. McEvoy, A. Shmeliov, G. S. Duesberg, J. N. Coleman, Y. Gogotsi and V. Nicolosi, *Adv Mater*, 2017, **29**.